J Solid State Electrochem (2012) 16:297–304
DOI 10.1007/s10008-011-1327-6

ORIGINAL PAPER

Synthesis and electrochemical capacitive behaviors of Co_3O_4 nanostructures from a novel biotemplating technique

Liangyu Gong · Xiaohong Liu · Linghao Su · Longqiang Wang

Received: 19 December 2010 / Revised: 28 January 2011 / Accepted: 30 January 2011 / Published online: 22 February 2011

Abstract A novel approach is developed to synthesize Co_3O_4 nanoparticles utilizing sawdust as a bio-template. Sawdust was first infiltrated with cobalt dichloride aqueous solution, and then, in situ precipitation reaction took place when different precipitators (NaOH or $H_2C_2O_4$) were added. Finally, the precursors, $Co(OH)_2$ and CoC_2O_4, were calcined to produce the final Co_3O_4 nanoparticles and the template was removed simultaneously. The structure and morphology of the obtained products were characterized by X-ray diffraction, Fourier transform infrared spectroscopy, and transmission electron microscopy. The observations revealed the formation of cubic phase Co_3O_4 with the average diameter of about 40 and 60 nm, respectively. Their electrochemical properties were investigated by cyclic voltammetry and galvanostatic charge–discharge tests. The highest specific capacitance of 289.7 $F g^{-1}$ for the obtained Co_3O_4 electrode was obtained even at a discharge current of 20 mA after the 100th cycle and it increased by about 4% after the 1,000th cycle, demonstrating good electrochemical stability of such electrode materials.

Keywords Co_3O_4 nanoparticles · Sawdust template · Electrochemical properties

Introduction

Supercapacitors have become one of the hottest research topics in energy storage and conversion systems because of their high power density and long cycle life and are being considered for a variety of applications such as in hybrid electric vehicles, uninterrupted power supplies, memory protection of computer electronics, and cellular devices [1, 2]. The synthesis of electrode materials with high performance is indispensable for developing an advanced supercapacitor device [3, 4], and three major types of electrode materials including carbon materials [5], conducting polymers [6] and transition metal oxides [7–14] are explored. Transition metal oxides, such as RuO_2 [7, 8], NiO [9], Co_3O_4 [10, 11], V_2O_5 [12], and MnO_2 [13, 14], have attracted great attention as capacitive materials since the 1990s. Among all these metal oxides, RuO_2 has an excellent ability to provide enough high specific capacitance [7, 8], but it is too expensive to use widely in commercialization [15]. Therefore, the alternative electrode materials should be inexpensive and exhibit capacitive behaviors similar to that of RuO_2.

Nanostructured Co_3O_4 materials are deemed to be one promising candidate due to its environmental friendliness, relatively low cost, high redox activity, high theoretical capacitance, and favorable electrochemical reversibility [16, 17]. Presently, various approaches including the template method [10, 11, 15, 18, 19], sol-gel process [20], chemical deposition [21], electrochemical precipitation [16], radio frequency sputtering [22], successive ionic layer adsorption and reaction [23], and spray pyrolysis [24] have been employed to fabricate Co_3O_4 nanoparticles with pseudocapacitive properties. Although different fabrication strategies have been employed for the synthesis of nanoscaled Co_3O_4 for pseudocapacitors, most of the preparation methods need either complicated technique or rigorous conditions. Therefore, it is still a challenge to explore simple methods for the fabrication of Co_3O_4 nanostructure for the application in pseudocapacitors.

L. Gong · X. Liu · L. Su (✉) · L. Wang
College of Chemistry and Pharmaceutical Sciences,
Qingdao Agricultural University,
Qingdao, Shandong 266109, People's Republic of China
e-mail: lygong@163.com

Herein, we report a facile synthesis technique to obtain Co_3O_4 nanoparticles for pseudocapacitors using cheap, abundant, and reproducible sawdust as a template. Compared with other hard or soft template methods [10, 11, 15, 18, 19], such a biotemplating technique provides a convenient and cheap way. To the best of our knowledge, there has been no report on the synthesis of Co_3O_4 nanoparticles for pseudocapacitors with the assistance of sawdust. Moreover, the electrochemical properties were investigated by the techniques of cyclic voltammetry and galvanostatic charge–discharge. It is found that the specific capacitance of Co_3O_4 electrode can be up to 289.7 Fg^{-1} even at a discharge current of 20 mA after the 100th cycle and can exhibit good long cycle life, demonstrating its good electrochemical stability.

Experimental

Treatment of the sawdust template

The sawdust used was obtained from phoenix tree branch. After sieving, the sawdust with particle size varying from 0.3 to 2 mm was pretreated in 10% NaOH solution by ultrasonication for 3 h, then washed with deionized water and dried at 60 °C for 24 h.

Synthesis of Co_3O_4

All chemicals used in this study were in analytical grade and used without further treatment. In a typical procedure, 1 g of the alkali-treated sawdust was dispersed in 20 ml 1 mol L^{-1} $CoCl_2$ solution under stirring at 60 °C for 72 h. After aging for several hours, the clear supernatant solution was siphoned off and an appropriate amount of a precipitator (40 ml 1 mol L^{-1} NaOH aqueous solution or 0.5 mol L^{-1} $H_2C_2O_4$ aqueous solution) was added dropwise into the remainder with vigorous stirring until a dark precipitate was formed. The obtained precipitates ($Co(OH)_2$/sawdust and CoC_2O_4/sawdust composite) were centrifuged, washed with deionized water and ethanol for several times, and calcined at 500 °C for 3 h. For the sake of simplicity, Co_3O_4 samples obtained by calcination of the $Co(OH)_2$/sawdust and CoC_2O_4/sawdust composite were labeled as Co-1 and Co-2, respectively. In order to investigate the template effect, control experiments were carried out in which only sawdust was omitted and the obtained samples from direct thermal decomposition of $Co(OH)_2$ and CoC_2O_4 precursor were designated as Co-3 and Co-4, respectively.

Characterizations

The X-ray diffraction (XRD) patterns of the obtained samples were recorded on a Bruker D8 Advance-X diffractometer (Germany) with Cu Kα radiation (λ= 0.15418 nm). Fourier transform infrared (FT-IR) spectra of the samples were obtained on a Nicolet IR200 spectrometer using KBr slice (sample/KBr=1:100 weight ratio). The transmission electron microscopy (TEM) images were recorded on a FEI Tecnai G^2 20-TWIN microscope operating at an acceleration voltage of 200 kV. Thermogravimetric and differential thermal analysis (TG/DTA) of the precursors were carried out on a Henven HGT-1 thermal analyzer at a heating rate of 10 °C min^{-1} under air atmosphere.

Electrochemical tests

The fabrication of working electrodes was carried out as follows. Briefly, the active materials Co_3O_4, acetylene black, and polyterafluoroethlene were mixed in a mass ratio of 70 : 25 : 5, dispersed in ethanol, and then pressed (20 MPa) onto a current collector of a nickel foam (1 cm^2). A three-electrode single-cell system at room temperature was used for all electrochemical measurements and 6 mol L^{-1} KOH aqueous solution was used as electrolyte. The platinum plate and Ag/AgCl electrode were used as the counter and reference electrodes, respectively. Cyclic voltammetry (CV) measurements were performed on a LK2005A-style electrochemical workstation. The galvanostatic charge–discharge performance of the electrodes was evaluated with a Land CT2001A battery program-control test system.

Results and discussion

TG/DTA analysis

The differential thermal analysis (DTA) and thermogravimetric analysis (TG) curves of the sawdust and the composites are listed in Fig. 1. Figure 1a shows the TG/DTA profiles of just the sawdust, a weight loss of ca. 100% was observed below 540 °C, indicating the sawdust was totally converted to CO_2 and H_2O. The cobalt hydroxide/sawdust composite shows two weight loss steps with increasing temperature (Fig. 1b). The first step observed at 20–180 °C corresponds to the removal of adsorbed water and interlayer water and the associated weight loss was 5.3%. The second weight loss step at 180–450 °C can be attributed to decomposition of the sawdust and cobalt hydroxide and the weight loss was 37.4%. There was a broad DTA peak at around 180–450 °C, which resulted from the decomposition of the cobalt hydroxide/sawdust composite. Figure 1c gives the TG/DTA curves of the cobalt oxalate/sawdust composite, which also shows two weight loss steps. The first stage involving dehydration occurred at around 20–220 °C and the associated weight

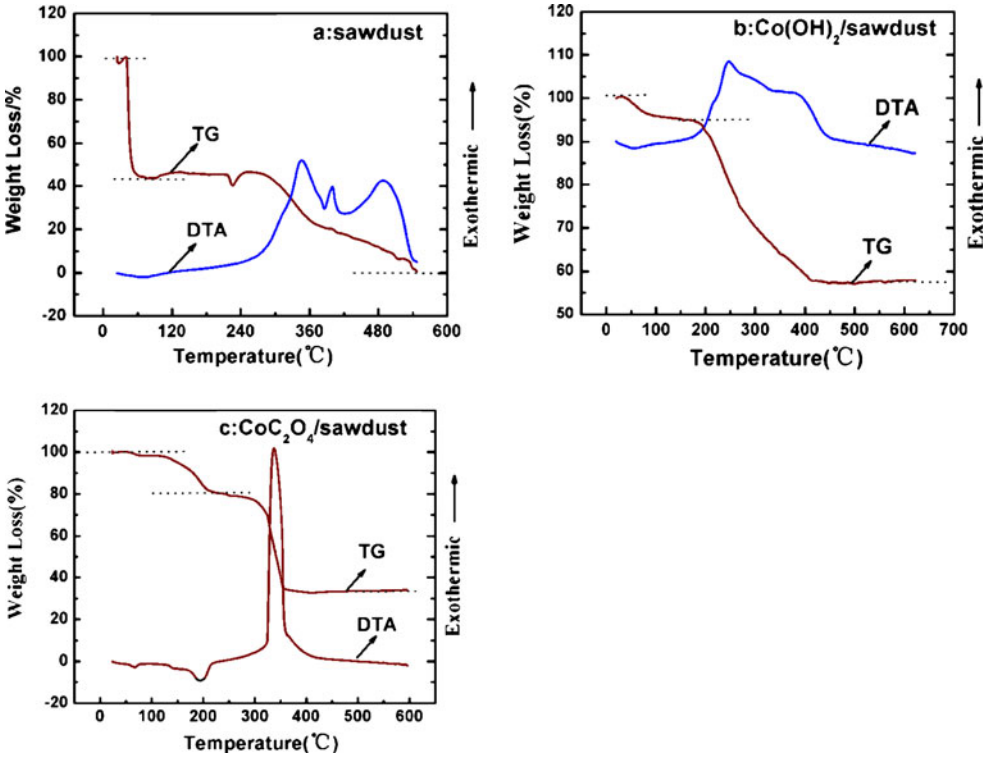

Fig. 1 TG and DTA curves for the thermal decomposition of **a** sawdust, **b** $Co(OH)_2$/sawdust composite, and **c** $Co_2C_2O_4$/sawdust composite

loss was 16.1%. As the temperature increased, a well-defined DTA peak due to the decomposition of cobalt oxalate/sawdust appeared at around 220–420 °C and was accompanied by a weight loss of 53.1% in TG curves. From these results, 500 °C appears to be the optimum calcination temperature for the composites.

FT-IR analysis

Figure 2 provides the FT-IR spectra for the samples before and after calcination. Compared with the spectrum of the sawdust (Fig. 2a), the characteristic band for O–H of the cobalt hydroxide at 3,629.47 cm^{-1} is clearly observed in

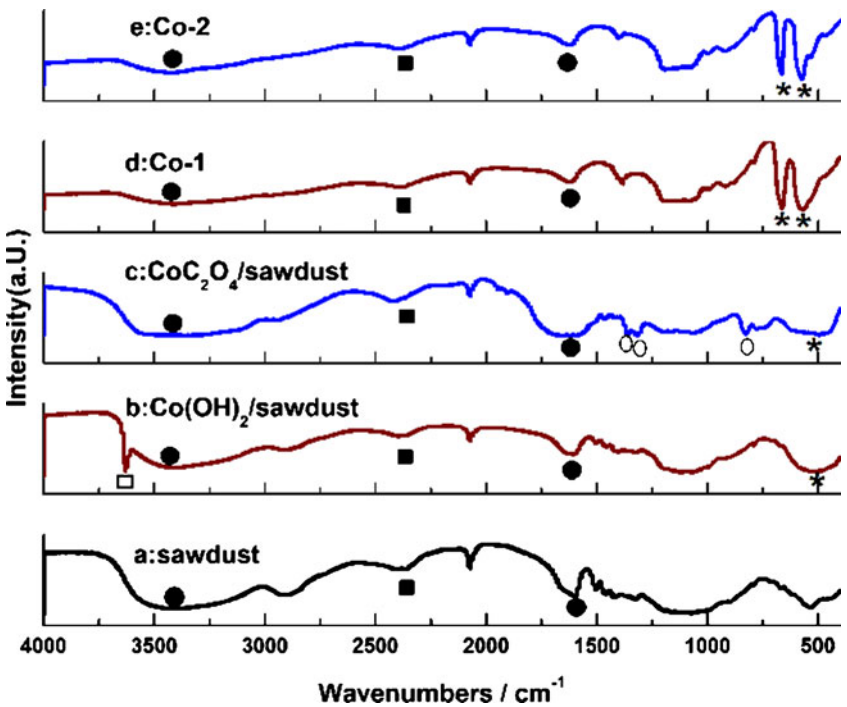

Fig. 2 **a**–**e** FT-IR spectra of sawdust, CoC_2O_4/sawdust, $Co(OH)_2$/sawdust hybrid precursors and the final Co_3O_4 products

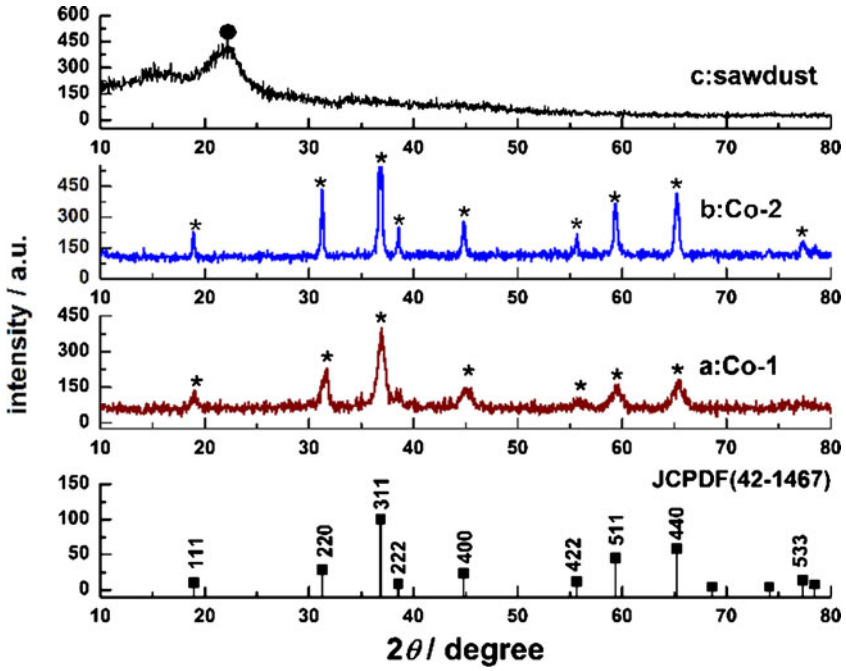

Fig. 3 **a**–**c** XRD patterns of cubic Co_3O_4 samples and the sawdust

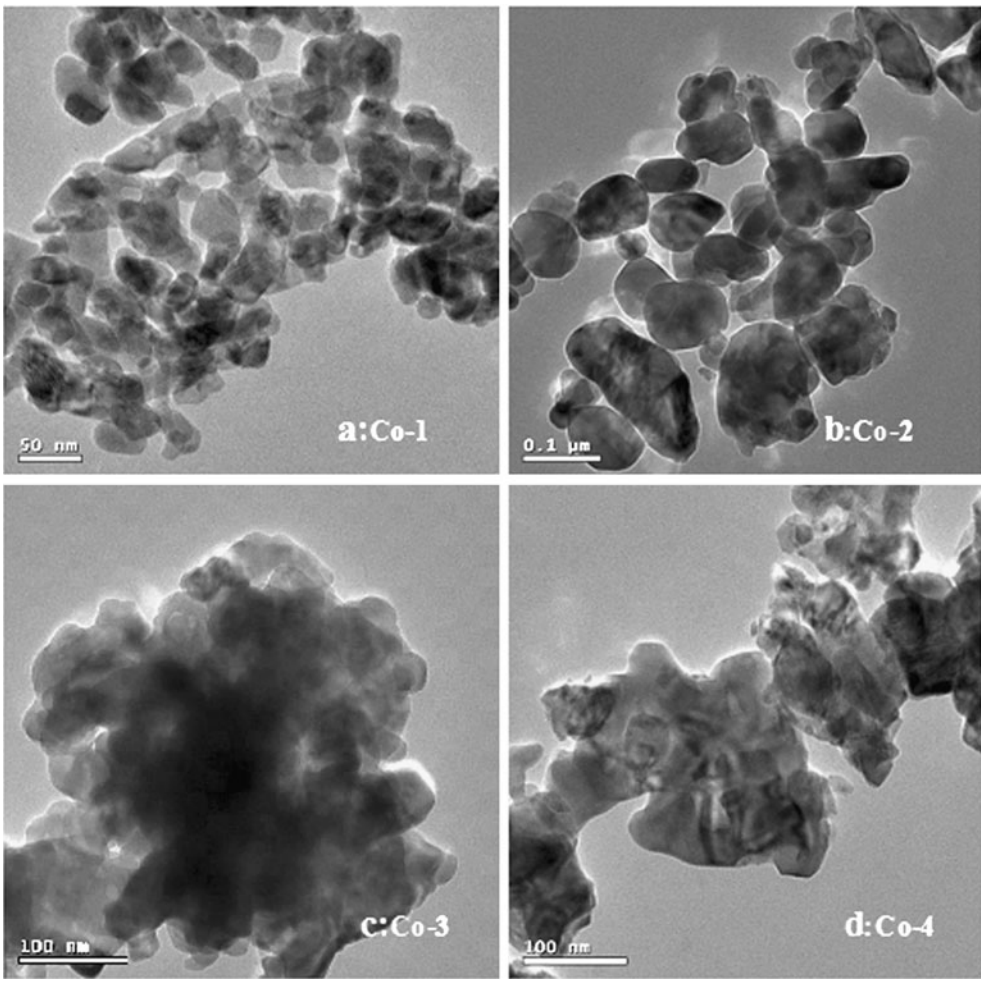

Fig. 4 TEM images of the as-prepared sample Co-1 (**a**), Co-2 (**b**), Co-3 (**c**), and Co-4 (**d**)

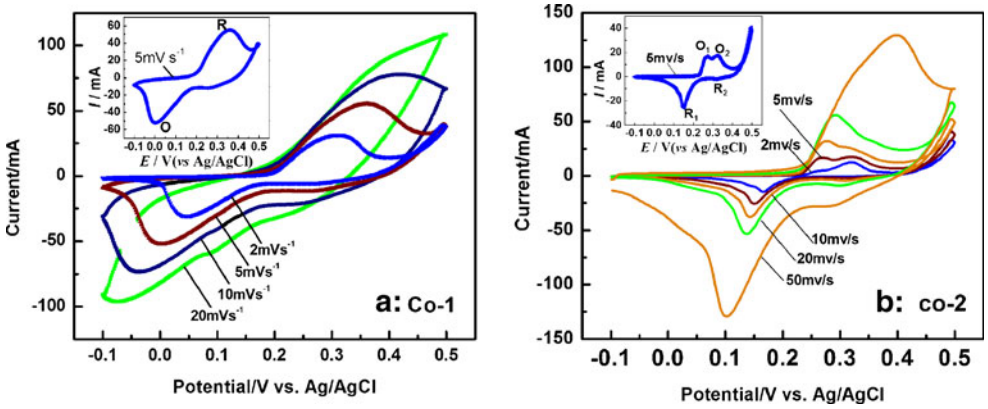

Fig. 5 CV curves of Co-1 (**a**) and Co-2 (**b**) at different scan rates of 2, 5, 10, 20, and 50 mV s^{-1} in 6 mol L^{-1} KOH electrolyte. *Insets*: CV curves at 5 mV s^{-1}

Fig. 2b, accompanied with the bending vibration band for free Co-OH group at 529.18 cm^{-1} [25, 26]. The closely spaced bands at 1,360.24 and 1,316.40 cm^{-1} depicted in Fig. 2c, which are assigned to symmetric γ(C–O), indicate the presence of bridging oxalates with all four oxygen atoms coordinated to the metal atoms. In addition, the asymmetric δ(O–C–O) band appears at 826.06 cm^{-1}, while the broad band at 494.30 cm^{-1} is assigned to γ(Co–O) and symmetric δ(C–C–O) [27]. It is therefore confirmed that the $Co(OH)_2$ and CoC_2O_4 are successfully formed and functionalized with sawdust, respectively. After sintering at 500 °C, the characteristic absorption bands of all the above mentioned peaks of $Co(OH)_2$ and CoC_2O_4 disappear, and the absorption peaks at ca. 662.29 and 570.28 cm^{-1} corresponding to the ν(Co-O) modes of Co_3O_4 appear in Fig. 2d, e, indicating the formation of Co_3O_4 nanocrystals [27–29]. Notably, there always exist the broad bands centered at ca. 3,400.08 cm^{-1} and the peaks at ca. 1,630.67 cm^{-1} in Fig. 2a–e, which should be assigned to the O–H stretching and bending modes of water, respectively [21, 29–31]. The peaks at ca. 2,398.87 cm^{-1} should be assigned to CO_2 vibration by environmental or personal factors [27, 29].

XRD analysis

The powder XRD patterns of sawdust and the resulting Co_3O_4 samples are shown in Fig. 3. Patterns a and b clearly exhibit the typical diffraction peaks of Co_3O_4 at 2θ values of 19.0°, 31.1°, 36.8°, 38.6°, 44.8°, 55.6°, 59.3°, and 65.2°, corresponding to (111), (220), (311), (222), (400), (422), (511), and (440) planes, respectively, which perfectly agrees with a cubic phase structure of Co_3O_4 (JCPDS Card No. 42-1467). In addition, it should be noted that the peak located at a 2θ value of about 23° which is referred to sawdust is not detected in Co_3O_4 samples. All these results indicated that the precursors were thoroughly converted into Co_3O_4 nanoparticles and the sawdust was removed completely after the calcinations at 500 °C, which is consistent with the FT-IR observations.

Morphology analysis

Figure 4 shows the TEM images of the as-prepared samples, and it can be found that the irregular spherical Co_3O_4 samples with an average diameter of 40 nm for Co-1 and 60 nm for Co-2 were obtained, respectively. As for the

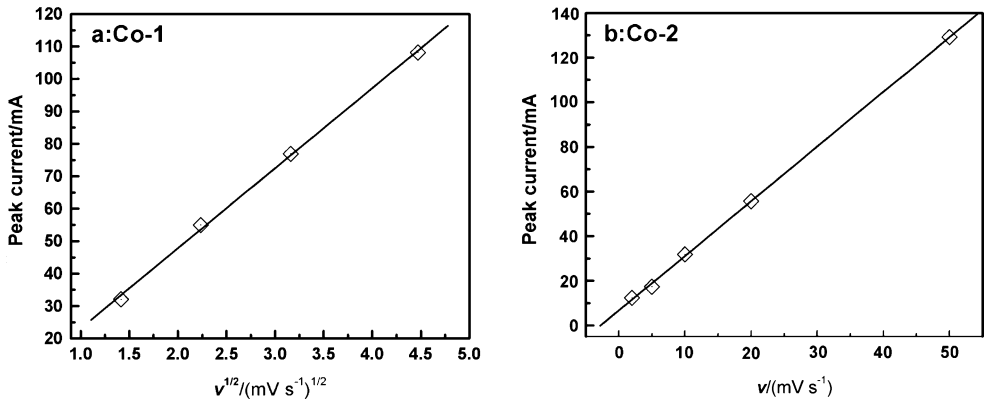

Fig. 6 Dependence of the peak current (i) on the square root of the scan rate ($v^{1/2}$) for the Co-1 electrode (**a**) and on the scan rate (v) for the Co-2 electrode (**b**)

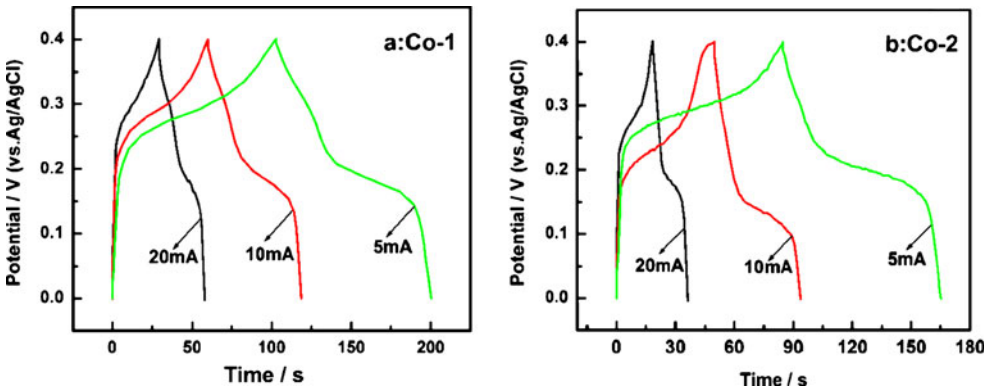

Fig. 7 Typical charge–discharge curves of Co-1 (**a**) and Co-2 (**b**) at the 100th cycle. The tests were performed at the galvanostatic current of 5, 10, and 20 mA within the potential window of 0 to 0.4 V (vs. Ag/AgCl) in 6 mol L^{-1} KOH electrolyte, respectively

formation of spherical Co_3O_4 nanoparticles, it can be attributed to the restriction functions of the cavity of sawdust. Firstly, the Co^{2+} was adsorbed on the surface of the inner cavity in the sawdust in the immersing process. Then, in situ precipitation reaction took place when the NaOH or $H_2C_2O_4$ solution was added dropwise, which is confirmed by the FT-IR results. In the process of aging, the resulting precipitate, $Co(OH)_2$ or CoC_2O_4, was inclined to grow and extend to the center of the inner cavity gradually until the inner cavity was fully filled with the precipitate. Owing to the confinement effect of the sawdust template, $Co(OH)_2$ or CoC_2O_4 transformed into Co_3O_4 nanoparticles in the subsequent calcination process and sawdust was removed simultaneously. Moreover, the samples Co-3 and Co-4 both exhibit agglomerated irregular-shaped particles (Fig. 4c, d), which demonstrate that the sawdust plays a crucial role in the formation of Co_3O_4 nanoparticles.

Electrochemical properties

Figure 5 depicts the CV curves of samples Co-1 (a) and Co-2 (b) at different scan rates of 2, 5, 10, 20, and 50 mV s^{-1} in 6 mol L^{-1} KOH electrolyte, respectively. The obvious deviation of the shapes of CVs from the ideal rectangular shape revealed that the capacitive characteristic of the as-prepared Co_3O_4 samples is different from that of electric double-layer capacitance, but faradic capacitance, which mainly originates from the redox reaction. A pair of broad redox peaks labeled as R and O can be seen within the potential range of −0.1–0.5 V for sample Co-1(Fig. 5a), indicating that reversible and continuous faradic redox reactions of Co_3O_4 are involved during the charge and discharge processes. The electrochemical reaction scheme is proposed as follows [32, 33]:

$$Co_3O_4 + OH^- + H_2O \leftrightarrow 3CoOOH + e^-$$

The curve is more symmetric at low scan rate. As the scan rate increases, the profiles become gradually distorted. This may be caused by an effective ion transport into the pores of active materials and small concentration polarization at low scan rate, while at a higher scan rate, some active surface areas are inaccessible for charge storage and big concentration polarization easily appeared [34]. In the typical CVs for the sample Co-2, two pairs of well-resolved redox peaks labeled as R_1, R_2, O_1, and O_2 can be observed (Fig. 5b). Peaks O_1 and O_2 represent the conversion processes of $Co^{2+} \rightarrow Co^{3+}$ and $Co^{3+} \rightarrow Co^{4+}$, and peaks R_1 and R_2 represent the corresponding inverse processes, respectively [10, 11]. Besides, the peak currents increase with increasing scan rate under the same potential both for samples

Table 1 The specific capacitance of the as-prepared Co_3O_4 after the 100th cycle at different currents in 6 mol L^{-1} KOH electrolyte

Sample	Specific capacitance (F g^{-1}) at different currents		
	5 mA	10 mA	20 mA
Co-1	243.4	293.3	289.7
Co-2	201.3	218.6	179.1

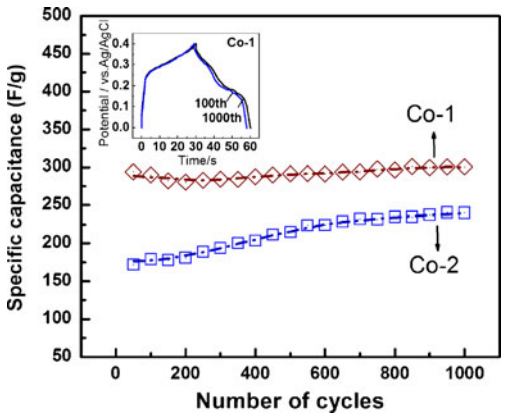

Fig. 8 Variations of the specific capacitance of the Co-1 and Co-2 electrodes as a function of cycle number and the corresponding charge–discharge curves of the Co-1 electrode at the 100th and the 1,000th cycles (*inset*). The charge–discharge tests were performed at the galvanostatic current of 20 mA within the potential window of 0 to 0.4 V (vs. Ag/AgCl) in 6 mol L^{-1} KOH electrolyte

Co-1 and Co-2, which is due to the rapid reversible redox reaction that occurred among the electrode materials [34].

Figure 6a further shows that the cathodic peak current of the Co-1 electrode is in proportion to the square root of the scan rate, indicating that the corresponding reaction kinetics is controlled by the diffusion process [18, 35], while a good linear relationship was observed between the anodic peak current of the Co-2 electrode and the scan rate (Fig. 6b), suggesting that the interface reaction of Co-2 electrode is one adsorption-controlled process. The difference between Co-1 and Co-2 may lead to their capacitive disparity.

The charge–discharge curves at the 100th cycle of the Co_3O_4 samples in 6 mol L^{-1} KOH electrolyte at the constant current of 5, 10, and 20 mA in the potential range of 0 to 0.4 V (vs. Ag/AgCl) are shown in Fig. 7. Obviously, all the discharge curves of sample Co-1 (Fig. 7a) and sample Co-2 (Fig. 7b) are not linear, indicating that the capacitive performance is not pure electric double-layer capacitance, but faradic capacitance, which is in agreement with CVs in Fig. 5. The curves consist of two sections, a sudden potential drop (0.4–0.2 V) followed by a slow potential decay (0.2–0 V). The first potential drop results from the internal resistance, and the subsequent potential decay represents the pseudocapacitance feature arising from the electrochemical adsorption–desorption or redox reaction at an interface between the electrode and the electrolyte [36, 37]. The capacitance value can be calculated from the discharge curves according to the following equation:

$$C_{\mathrm{p}} = \frac{I \times t}{m \times \Delta V}$$

Here, C_{p} is the specific capacitance, I is the discharge current, t is the discharge time, ΔV is the potential change during discharge, and m is the mass of the active material within the work electrode. The calculated specific capacitance values of the as-prepared Co_3O_4 samples after the 100th cycle at the constant current of 5, 10, and 20 mA, respectively, are listed in Table 1. As can be seen from Table 1, the specific capacitance of Co-1 is slightly higher than that of Co-2. The highest specific capacitance of 289.7 $F g^{-1}$ for the obtained Co_3O_4 electrode is obtained even at the discharge current of 20 mA after the 100th cycle.

Since long cycle life of supercapacitors is a crucial parameter for their practical applications, the cyclic charge–discharge tests were employed to examine the service life of the Co_3O_4 electrodes and the corresponding results are shown in Fig. 8. The electrodes exhibit good capacitance retention after 1,000 cycles even at the constant current of 20 mA. Interestingly, the specific capacitance of the samples increased with cycle numbers, instead of decreasing as reported in most cycle life tests, which demonstrated that the Co_3O_4 electrodes exhibit good cycle stability and a very high degree of reversibility in the repetitive charge/discharge cycles. As for the Co-1 electrode, for example, its charge–discharge curve for the 100th cycle is almost same as that for the 1,000th cycle (see inset in Fig. 8) and the specific capacitance for the 1,000th cycle increases by about 4%.

Conclusions

Co_3O_4 nanoparticles were successfully fabricated via a simple, low cost, practical, and environment-friendly synthesis route with sawdust as the bio-template. The XRD and FT-IR analysis demonstrate that the products are cubic structure Co_3O_4, and TEM reveals that the as-synthesized Co_3O_4 bears the irregular morphology with an average diameter of 40 or 60 nm when NaOH and $H_2C_2O_4$ were used as precipitators, respectively. The formation of Co_3O_4 nanoparticles mainly ascribes to the porous structure of sawdust. Through electrochemical characterizations, the materials exhibit the promising application properties for a supercapacitor, including strong reversibility, high specific capacitance, and good stability.

Acknowledgments The work was financially supported by the Natural Science Foundation of China (30871894) and the Outstanding Young Scientists Incentive foundation of Shandong Province (BS2010NJ007).

References

1. Kotz R, Carlen M (2000) Electrochim Acta 45:2483–2498
2. Subramanian V, Zhu HW, Vajtai R, Ajayan PM, Wei BQ (2005) J Phys Chem B 109:20207–20214
3. Yang GW, Xu CL, Li HL (2008) Chem Commun 48:6537–6539
4. Hu CC, Chang KH, Lin MC, Wu YT (2006) Nano Lett 6:2690–2695
5. Bao QL, Bao SJ, Li CM, Qi X, Pan CX, Zang JF, Lu ZS, Li YB, Tang DY, Zhang S, Lian K (2008) J Phys Chem C 112:3612–3618
6. Mi HY, Zhang XG, Ye XG, Yang SD (2008) J Power Sources 176:403–409
7. Zheng JP, Jow TR (1995) J Electrochem Soc 142:L6–L8
8. Zheng JP, Cygan PJ, Jow TR (1995) J Electrochem Soc 142:2699–2703
9. Yuan CZ, Gao B, Su LH, Zhang XG (2008) Solid State Ion 178:1859–1866
10. Wang L, Liu XH, Wang X, Yang XJ, Lu LD (2010) Curr Appl Phys 10:1422–1426
11. Cui L, Li J, Zhang XG (2009) J Appl Electrochem 39:1871–1876
12. Lee HY, Goodenough JB (1999) J Solid State Chem 148:81–84
13. Subramanian V, Zhu HW, Wei BQ (2006) J Power Sources 159:361–364
14. Jiang RR, Huang T, Liu JL, Zhuang JH, Yu AS (2009) Electrochim Acta 54:3047–3052
15. Liu Y, Zhao WW, Zhang XG (2008) Electrochim Acta 53:3296–3304
16. Srinivasan V, Weidner JW (2002) J Power Sources 108:15–20
17. Deng MJ, Huang FL, Sun IW, Tsai WT, Chang JK (2009) Nano. 20: 175602

18. Li YH, Huang KL, Liu SQ, Yao ZF (2011) J Solid State Electrochem
19. Ji GB, Gong ZH, Zhu WX, Zheng MB, Liao ST, Shen K, Liu JS, Cao JM (2009) J Alloy Compd 476:579–583
20. Lin C, Ritter JA, Popov BN (1998) J Electrochem Soc 145:4097–4103
21. Kandalkar SG, Dhawale DS, Kim CK, Lokhande CD (2010) Synth Met 160:1299–1302
22. Kim HK, Seong TY, Lim JH, Cho WI, Yoon YS (2001) J Power Sources 102:167–171
23. Kandalkar SG, Gunjakar JL, Lokhande CD (2008) Appl Surf Sci 254:5540–5544
24. Shinde VR, Mahadik SB, Gujar TP, Lokhande CD (2006) Appl Surf Sci 252:7487–7492
25. Gupta V, Kusahara TK, Toyama HS, Gupta SH, Miura N (2007) Electrochem Commun 9:2315–2319
26. Jayashree RS, Kamath PV (1999) J Mater Chem 9:961–963
27. Ren L, Wang PP, Han YS, Hu CW, Wei BQ (2009) Chem Phys Lett 476:78–83
28. Zou DB, Xu C, Luo H, Wang L, Ying TK (2008) Mater Lett 62:1976–1978
29. Sun LG, Li HF, Ren L, Hu CW (2009) Solid State Sci 11:108–112
30. Wang Y, Yang WS, Chen C, Evans DG (2008) J Power Sources 184:682–690
31. Ai LH, Jiang (2009) J Powder Technol 195:11–14
32. Deng JJ, Deng JC, Liu ZL, Deng HR, Liu B (2009) J Mater Sci 44:2828–2835
33. Deng JJ, Deng JC, Liu ZL, Deng HR, Liu B (2009) J Solid State Electrochem 13:1387–1394
34. Luo JM, Gao B, Zhang XG (2008) Mater Res Bull 43:1119–1125
35. Wang CH, Du HY, Tsai YT, Chen CP, Huang CJ, Chen LC, Chen KH, Shih HC (2007) J Power Sources 171:55–62
36. Tao F, Zhao YQ, Zhang GQ, Li HL (2007) Electrochem Commun 9:1282–1287
37. Li YH, Huang KL, Zeng DM, Liu SQ, Yao ZF (2010) J Solid State Electrochem 14:1205–1211